Essential Readings in Light Metals: Cast Shop for Aluminum Production.
Edited by John F. Grandfield and Dmitry G. Eskin.

Zr-POISONING OF GRAIN REFINER PARTICLES STUDIED IN Al-Ni-Zr AMORPHOUS ALLOYS

P. Schumacher, P. Cizek
Department of Materials
University of Oxford
Parks Rd, Oxford, OX1 3PH, U.K.

A.M. Bunn
Department of Materials Science and Metallurgy
University of Cambridge
Pembroke Street, Cambridge, CB2 3QZ, U.K.

Abstract

The poisoning mechanism of Zr was investigated using a metallic glass technique. Grain refining particles from a 5:1 TIBAL rod were embedded into a metallic glass produced by melt-spinning an $Al_{87}Ni_{10}Zr_3$ (at.%) alloy. Within the as-quenched samples, dendrites of α-Al were found on TiB_2 particles and on primary dendrites of Al_3Zr competing to nucleate α-Al. On boride particles a thin diminishing tri-aluminide layer was found to nucleate α-Al. Zr was found to preferentially diffuse into TiB_2 particles rather than to form a thick layer of Al_3Zr on these particles. The epitaxial relationship found between the tri-aluminide layer and the $(Zr,Ti)B_2$ particle is limited by the expanding lattice parameter of the boride with increasing Zr content. The nucleation mechanism on the boride particles and the influences of Zr are discussed with respect to conventional casting practice.

Introduction

The control of grain size is of importance in Al products with little scope for further thermomechanical treatments, such as plate products. In particular, problems can be encountered in thick plate production of 7xxx series alloys for airframe applications where the presence of Zr leads to decreased performance of conventional TIBAl (5:1) grain refiner. The negative effects of Zr, and to a lesser extend that of Cr, on the grain refinement have been termed 'Zr-poisoning' and do not only affect grain size but may also affect macro-segregation. The effects of Zr poisoning are well documented [1-7] and concentrate on effects of growth restriction elements in connection with Zr [6,8] and effects on nucleation sites [1-5]. However, Bunn et al. [7] concluded that growth restriction effects are not the dominant factor in Zr poisoning. Further evidence that Zr poisoning is mainly affected by nucleation, is the remarkable absence of this poisoning effect when TiC refiner particles are used [9].

The kinetics of Zr poisoning have been demonstrated by Bunn et al. [7] to be temperature and time activated. In samples held at temperatures of 720, 760 and 800°C for up to 300 h under continuous stirring no decrease in refiner performance was found, while after 10 min of holding the subsequent addition of Zr resulted in poisoning after short times thereafter. Poisoning is further enhanced at higher temperatures and longer times. In commercial practice the refiner rod is added to the melt already containing Zr resulting in a time delay during which the refining rod dissolves into the melt before Zr-poisoning kinetics are activated.

The key to understand the poisoning mechanism and its kinetics is to elucidate the effect of Zr on the nucleation mechanism of α-Al. In particular, the role and stability of Ti in TiB_2 and Al_3Ti to

remain unaffected by a Zr substitution will affect the nucleation mechanism. Jones and Pearson [1] suggested that TiB_2 may be replaced by ZrB_2 while more recently Bunn et al. [7] found mixed $(Zr,Ti)B_2$ particles and discussed possible implications of lattice matching on adsorbed Al_3Ti layers on basal planes of mixed $(Zr,Ti)B_2$ particles.

Typical 7xxx series alloys contain high amounts of Zr (0.12 wt.%) for dispersion hardening. Consequently, during solidification the Zr levels become close to those corresponding to the peritectic horizontal when additional Ti from refiner rod is present and Al_3Zr may form as the primary phase. Al_3Zr exhibits a peritectic reaction with liquid to form Al at 660.8°C and could act a good nucleant for aluminium. The addition levels of Zr are much higher than those of Ti (0.01- 0.02 wt.%), which also exhibits a peritectic with liquid and Al_3Ti to form α-Al at a higher temperature (665°C) than Al_3Zr. A pseudobinary cut through both Al_3Ti and Al_3Zr [10] suggests that, up to 6.25 at.% Zr, Al_3Ti remains stable before $Al_3(Zr,Ti)$ is formed.

The complex potential nucleation mechanisms cannot be elucidated by conventional casting experiments, such as the TP1 test, in which nucleation is obscured by subsequent growth and impingement of crystals. A metallic glass technique, used successfully [11-15] to investigate the influence of excess Ti on the nucleation of α-Al, has been adapted in this work to be analogous to Zr poisoning conditions. Essentially, in this technique grain refining particles are added to a glass-forming melt similar (but richer in composition) to Al melts and containing Zr. On rapid quenching nucleation of α-Al occurs on the added refining particles when the melt is undercooled below the metastable extension of the Al liquidus. Growth of α-Al on the added particles is halted when the temperature decreases below the glass transition temperature. Subsequently, α-Al crystals nucleated on the refiner particles are embedded in a metallic glass and can be readily investigated in transmission electron microscopy. For the study of Zr poisoning a metallic glass-forming alloy $Al_{87}Ni_{10}Zr_3$ was chosen identical in composition to an earlier reported glass former without particle addition [16]. The effects of Zr on a previously found nucleation mechanism, in which a thin epitaxial Al_3Ti layer was preserved on TiB_2 faces readily nucleating α-Al only on basal faces [11-15], are studied with respect to di-borides and tri-aluminides which may form with Zr present. It is necessary to note that the metallic glass technique cannot simulate the effects of growth restriction on grain refinement but is ideally suited in the case of Zr poisoning where growth restriction effects appear to be negligible [7].

Experimental Methods

Pure elements of Al (99.999), Ni (99.99) and Zr (99.98) were used to produce ingots with a nominal composition of $Al_{87}Ni_{10}Zr_3$ (at.%) after repeated arc-melting in reduced (200 mbar) inert He atmosphere. After addition of 5:1 TIBAL grain refiner rod (London & Scandinavian Metallurgical Co Ltd) prior to melt-spinning, the overall composition was $(Al_{87-x}Ni_{10}Zr_3)_{100-y}+ (TiB_2)_y$ with $x = 0.05$ and $y = 0.16$ with the excess Al from the refiner rod to be subtracted from the nominal composition. Melt-spinning was in reduced (200 mbar) He atmosphere onto a rotating (50 m/s) copper wheel with close-loop controlled ejection temperatures of 1050, 1100 and 1150°C after holding times of 5 min. Ribbon samples were prepared for Differential Scanning Calorimetry (DSC, TA Instruments) and X-ray diffraction in a vertical diffractometer (Philips 1810). Thin foils were prepared by electro-polishing in 10 vol.% perchloric acid in ethanol at – 40°C and a voltage of ~ 20 V. Transmission electron microscopy (TEM) was performed using a Philips (CM20) microscope with attached energy-dispersive X-ray spectroscopy (LINK-EDS) at 200 keV.

Results and Discussion

As-quenched state

The variation in ejection temperature prior to melt-spinning has been designed to minimise the reaction kinetics of poisoning given the significantly higher temperatures than in conventional DC casting. The high temperatures were compensated by reduced holding times in the metallic glass experiment (5 min). Nevertheless, the lowest ejection temperature was limited by successful melting and subsequent vitrification of the alloy. XRD results of ribbons, spun from lower ejection temperatures, revealed substantial peaks (of Al, Al_3Zr and Al_3Ni) from crystallisation products occurring during quenching. Typical XRD traces are shown in Figure 1 for a ribbon successfully quenched from 1150°C and after subsequent annealing in DSC to 400°C. Despite significant peaks of Al and Al_3Zr in XRD traces, a broad halo characteristic for amorphous phase being present can be seen in Fig. 1(a). The remaining amorphous phase is solute enriched and devitrifies to the equilibrium phases Al_3Zr and Al_3Ni [16] on further annealing. Consequently, the work concentrated on the as-quenched samples melt-spun from 1150°C.

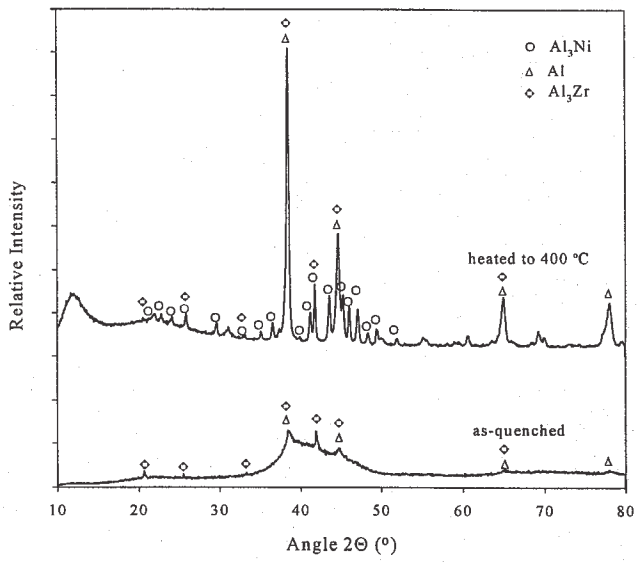

Figure 1: XRD trace of a ribbon quenched from 1150 °C showing broadening peaks for Al and some indication of Al_3Zr peaks (a) and after full transformation at 400 °C the equilibrium phases Al, Al_3Zr and Al_3Ni (b).

Quenched-in nuclei

During melt-spinning growth of crystals is strongly hindered in the glass-forming undercooled melt and recalescence is suppressed by high cooling rates. However, insufficient quench rates allowed other heterogeneous nucleation sites apart from borides to nucleate crystals. The crystalline peaks detected in

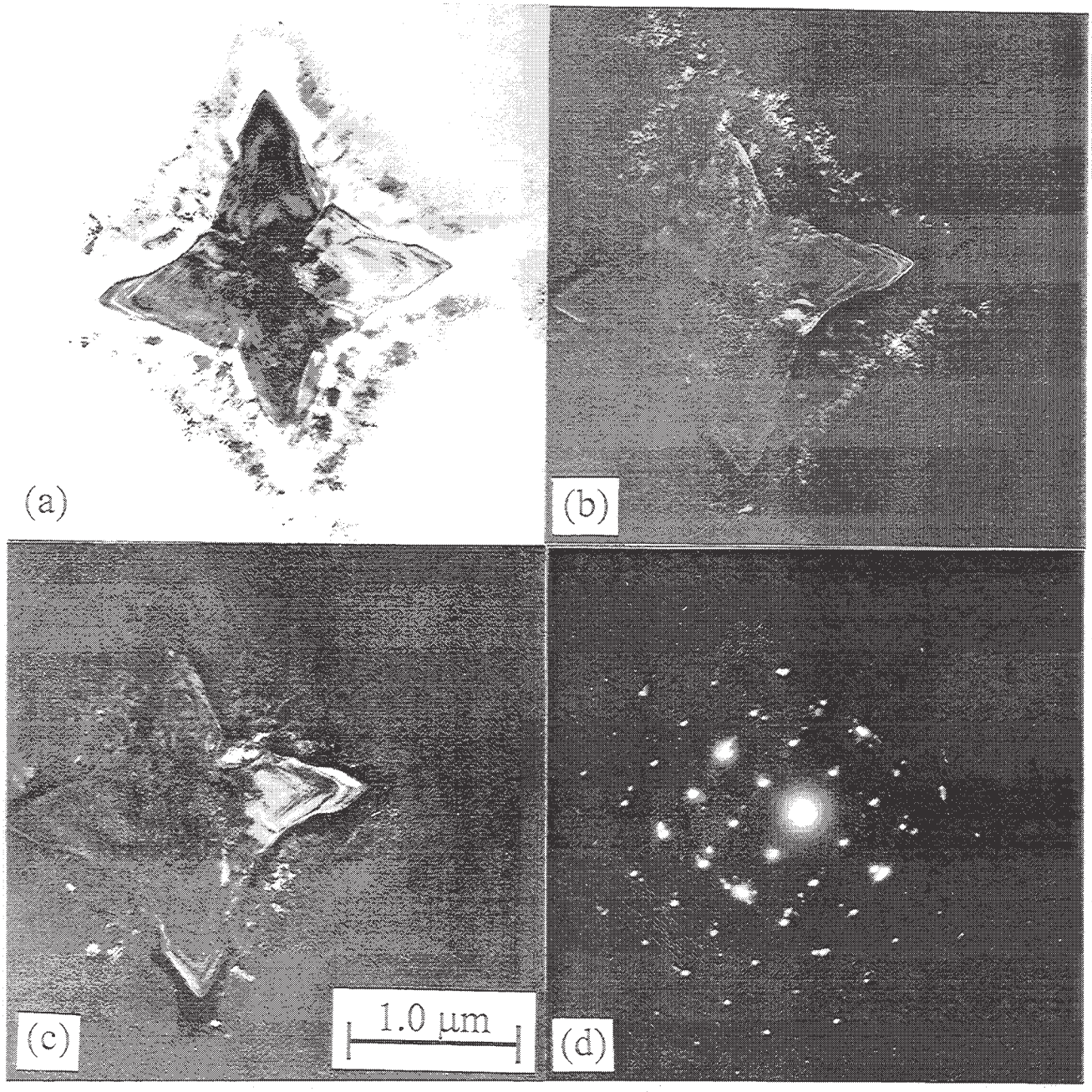

Figure 2: Bright-field TEM of Al_3Zr dendrite arms of different cubic orientation nucleating α-Al (a) and in dark-field TEM with the objective aperture on {002}Al spot (b) and on {002}Al_3Zr spot (c) and the complex corresponding selected area diffraction pattern (d).

XRD have been verified in TEM as dendrites of Al and Al_3Zr.

In Fig. 2, a well-defined dendritic structure with a four-fold symmetry can be seen in a bright-field TEM micrograph. The inserted selected area diffraction (SAD) pattern exhibits an ordered structure with a four-fold symmetry. Careful analysis of the diffraction pattern identifies the structure as being Al_3Zr with the electron beam close to the <001>Al_3Zr zone axis with overlapping weak <010> and <001>Al_3Zr zone axes from other cubic dendrite arms. The Al_3Zr dendrite is surrounded by smaller irregular dendrites growing on all faces exposed to the undercooled melt or subsequently on further cooling the metallic glass. Superimposed onto the <001>Al_3Zr diffraction pattern is a <001>Al pattern. The irregular Al dendrites exhibit an orientation relationship with the Al_3Zr dendrite and can be highlighted in dark-field TEM with the objective aperture on the {200}Al spots aligned with {200}Al_3Zr spots suggesting a cube to cube orientation relationship. However, different variants are possible

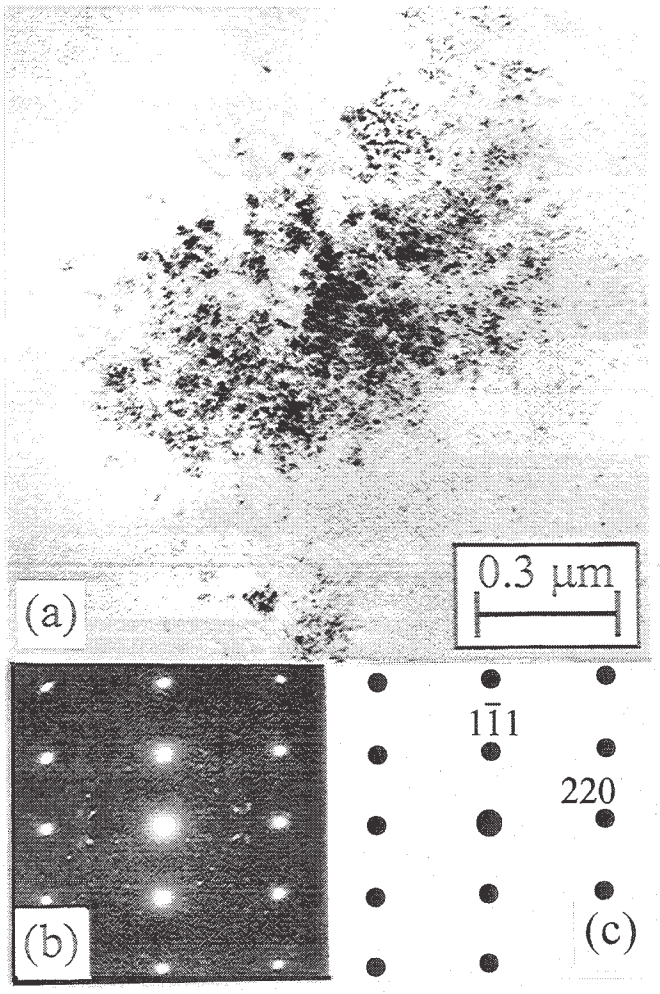

Figure 3: Bright-field TEM micrograph of a circular α-Al dendrite (a) and corresponding SAD pattern with the electron beam close to <112>Al zone axis (b).

on different parts of the Al_3Zr dendrite and not all of the α-Al dendrites appear light in dark-field TEM. Al_3Zr shows a peritectic reaction with liquid to form α-Al and it appears that the Al_3Zr crystals, nucleated and grown during insufficient quenching at a higher temperature, have nucleated α-Al on undercooling below the metastable extension of the Al-liquidus line. The irregular shape of the α-Al dendrites is similar to that observed in devitrification studies of a glass of identical composition [16] and suggests that the α-Al crystals were formed close to the glass transition temperature.

In Fig. 3, a separate α-Al dendrite tilted with its <112>Al zone axis close to the electron beam can be seen in bright-field TEM. Within the round shape of the dendrite, the possibility of a nucleation centre is indicated by additional spots in the SAD pattern suggesting heterogeneous nucleation of the α-Al. The most likely candidates are small Al_3Zr crystals described earlier, which nucleated and grew at a later stage compared to the larger Al_3Zr dendrites with a clearly developed dendritic shape.

Borides

Apart from the above described quenched-in nuclei, grain refining particles will also compete to nucleated α-Al. None of the separate Al_3Ti particles present in the refining rod have been found, consistent with the low (0.05 at.%) Ti concentrations at which they should dissolve. Some Ti is expected to be in solution in the Al_3Zr particle described above but was found to be below the detection limit of the EDS system. In contrast to the Al_3Ti particles, separate di-boride particles can be found embedded in the metallic glass matrix. In Fig. 4(a), a hexagonal boride platelet (crystallographically described as {h, k, . = - (h+k), l}) is viewed in bright-field TEM with its <11.0> zone axis close to the electron beam viewed with its basal plane edge-on. The inserted SAD pattern reveals weak streaking visible mainly on the 0-order spot in the <00.1> direction of the boride and an orientation relationship between the boride and the surrounding α-Al. In dark-field TEM in Fig. 4(b) the faceted nature of the boride can be seen on whose basal plane α-Al has nucleated. Careful dark-field TEM with the objective aperture on the 0-order spot streak reveals a weak layer (indicated by arrows in Fig. 4(d)) as found in earlier work on boride particles in metallic glasses not containing Zr. However, its crystallographic nature could not be identified from SAD patterns due to small size of the layer that appears to be inconsistent along the basal faces of the boride.

EDS analysis

EDS investigation was undertaken using spot analysis to overcome sample drift and to guarantee exact locations during measurements. Spot analysis was performed perpendicular to the basal faces of the hexagonal boride, tilted with its <11.0> or <10.0> zone axis close to being parallel with the electron beam. This insured a minimum overlap of phases at the interface of the boride with the aluminide and α-Al, and also avoided interference from diffraction at the interface. Despite the efforts to minimise errors in X-ray detection, significant amounts of background noise, visible in the form of CuK_α radiation, was detected. Therefore, only Zr above that in the amorphous matrix (3 at.%) was taken as having diffused into the boride. In Fig. 5, the spot analysis shows significant amounts of Zr above that of the matrix in the boride. Only little Ti could be detected within the boride particles, which suggests that Ti became almost completely replaced by Zr as found previously [7]. However, no significant amount of Zr was detectable in the aluminide layer, given the limitation of the EDS system used. In previous work [11,12] layer thickening was observed when elements soluble in Al_3Ti were added. This suggests that, under the present experimental conditions, all the Zr diffused into the boride rather than to thicken the aluminide layer.

Discussion and Conclusions

The marginal glass-forming ability of the alloy used, for the given processing conditions, did result in quenched-in nuclei of Al_3Zr and α-Al next to the added refiner particles. The dendritic nature of the Al_3Zr particles suggests insufficient quenching and/or insufficient melting prior to melt-spinning. Nevertheless, the Al_3Zr dendrites readily nucleated α-Al demonstrating that they are effective nucleation sites for α-Al, as previously shown by Marcantonio and Mondolfo [17] in conventional experiments. The Zr content of the alloy used in the present study was somewhat

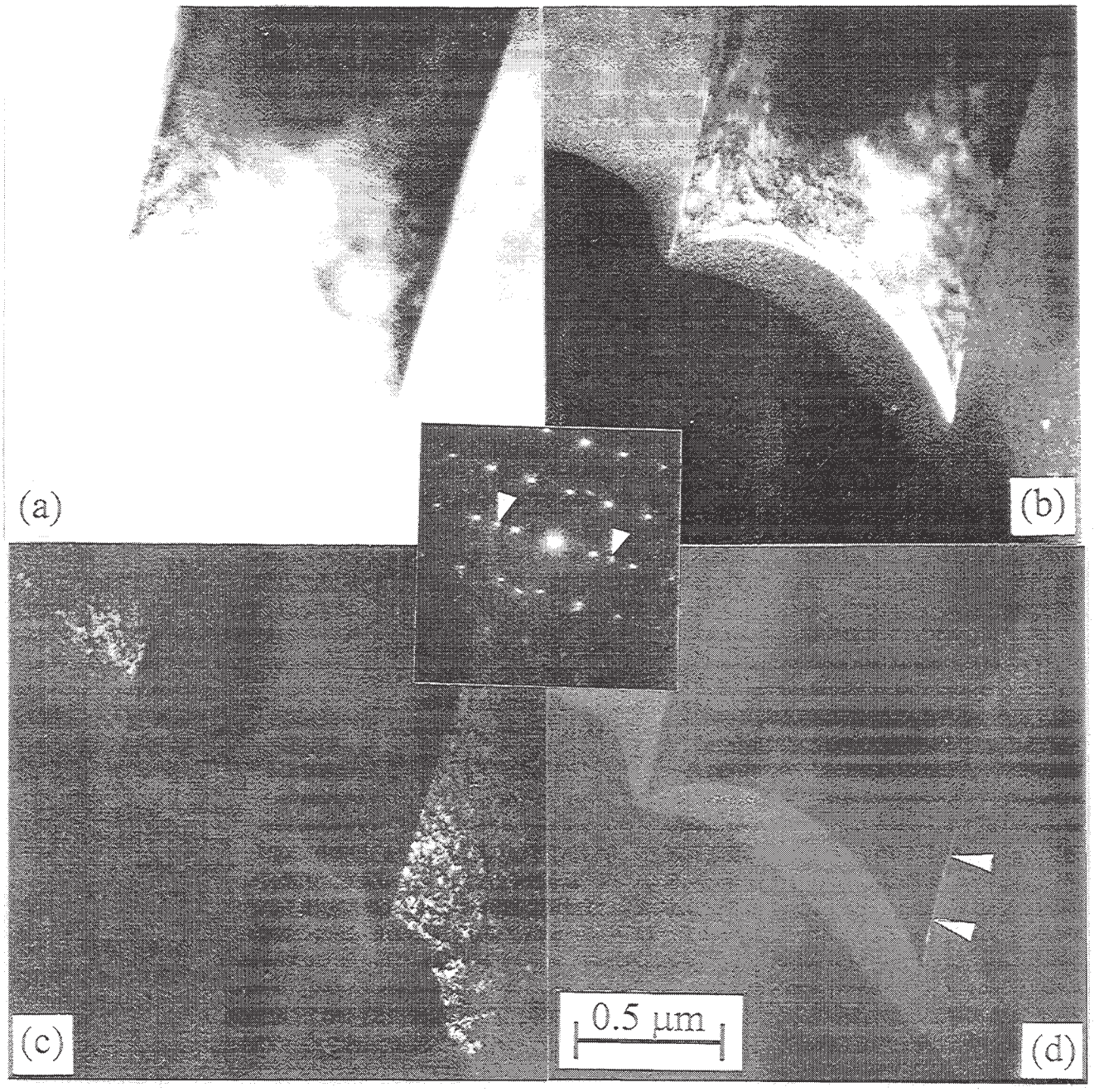

Figure 4: Bright-field TEM micrograph of a di-boride particle tilted with its <11.0> zone axis close to the electron beam (a) and dark-field TEM micrographs with the objective aperture on {00.1} di-boride (b), {111}Al (indicated by arrows in the diffraction pattern) (c) and on the weak streak close to 0-order spot (d).

higher, being hyper-peritectic, than in conventional Zr-containing alloys. In commercial casting practice, the formation of separate tri-aluminides is avoided if additional Ti concentrations are low. However, the crystallographic similarity between Al_3Zr and Al_3Ti suggests that they may share nucleation sites such as boride particles in previous work [11-14]. The difference in peritectic temperatures between Al_3Ti (665°C) and Al_3Zr (660.8°C) will make Al_3Ti the more potent nucleation site for α-Al but the number of Al_3Ti sites will be dependent on the phase equilibrium with Al_3Zr. Moreover, entrained droplet experiments of Al droplets in Al_3Ti [19] and Al_3Zr [20] seem to suggest that significant undercooling is possible in the case of Al_3Zr while there was no undercooling detectable for Al_3Ti making it an even more potent nucleation substrate.

In contrast to excess amounts of Ti or accidental Ta being present [11,12], the aluminide layer does not grow thicker when it is in contact with Zr. Zirconium energetically prefers to replace Ti in

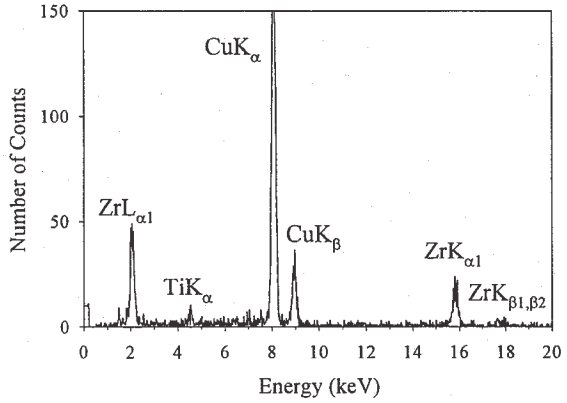

Figure 5: EDS-spot analysis of boride particle showing replacement of Ti by Zr in TiB_2.

the di-boride rather than to go into solution in the Al_3Ti layer or to form an Al_3Zr layer, despite Al_3Zr present in a bulk dendritic form elsewhere in the matrix. TiB_2 and ZrB_2 form a continuous solid solution [18] and any epitaxial layer of $Al_3(Ti,Zr)$ will be stretched by the larger lattice parameters of ZrB_2, as discussed by Bunn et al. [7], until the epitaxy cannot be maintained and the Al_3Ti layer vanishes and with it the capability to nucleate α-Al. The very thin and discontinuous layer in Fig. 4 exemplifies the above suggested mechanism and represents a snap shot at which Zr has started to diffuse into boride but has not yet let the layer vanish. In casting practice Zr poisoning should be overcome by late addition and short contact times of either grain refiner or a Zr containing pre-alloy with the melt. Thereby, aluminide layers present in the refiner rod [21] may remain stable for longer. Furthermore, it appears from conventional TP1 tests that, at lower temperatures, the kinetics of Zr poisoning are reduced and successful refinement can be achieved [7]. Future work will concentrate on identifying Zr contents within both the observed layers and di-borides using elemental EDS mapping, and potential influences of Cr on grain refinement, which interestingly exhibits a decreasing lattice parameter with increasing Cr content in $(Ti,Cr)B_2$ [18].

Acknowledgements

Pavel Cizek (GR\M12988), Alice Bunn (CASE-studentship 955564432) and Peter Schumacher (Advanced Fellowship AF/97/25440) are grateful for the support by the EPSRC and industrial support by London & Scandinavian Metallurgical Co Ltd, Rotherham, and Alcan International Ltd, Banbury.

References

[1] G.P. Jones and J. Pearson, Metall. Trans. B, 7B (1976) 223.
[2] W. Reif and W. Schneider, Giessereiforschung, 32 (1980) 53.
[3] M.E. Birch, in 'Aluminium-Lithium alloys III', (1986), 152, London, The Institute of Metals.
[4] A.A. Abdel-Hamid, Z. Metallkd., 80 (1989) 643.
[5] S.M. Ahmady, D.G. McCartney and S.R. Thistlethwaite, Light Metals 1990, (1990), p. 837, Warrendale, PA, TMS.
[6] M. Johnson, Z. Metallkd., 85 (1994) 786.
[7] A.M. Bunn, P. Schumacher, M.A. Kearns, C.B. Boothroyd and A.L. Greer, Mater. Sci. Techn., 15 (1999) 1115.
[8] J.A. Spittle and S.B. Sadli, Cast Met., 7 (1994) 247.
[9] P. Hoefs, W. Reif, A.H. Green, P.C van Wiggen, W. Schneider and D. Brandner, Light Metals 1997, ed. R. Huglen, (1997), p. 777, Warrendale, PA, TMS.
[10] S. Tsurekawa and M.E. Fine, Src. Metall., 16 (1982) 391.
[11] P. Schumacher and A.L. Greer, Mater. Sci. Eng. A, A178 (1994) 309.
[12] P. Schumacher and A.L. Greer, Mater. Sci. Eng. A, A181/182 (1994) 1335.
[13] P. Schumacher and A.L. Greer, Light Metals 1995, ed. J.W. Evans, (1995), p. 869, Warrendale, PA, TMS.
[14] P. Schumacher and A.L. Greer, Light Metals 1996, ed. W. Hale, (1996), p. 745, Warrendale, PA, TMS.
[15] P. Schumacher, A.L. Greer, J. Worth, P.V. Evans, M.A. Kearns, P. Fisher and A.H. Green, Mater. Sci. Techn., 14 (1998) 394.
[16] M. Blank-Bewersdorf, J. Mater. Sci. Lett., 10 (1991) 1225.
[17] J.A. Marcantonio and L.F. Mondolfo, J. Inst. Met., 98 (1970) 23.
[18] W.A. Zdaniewski, J. Am. Ceram. Soc., 70 (1987) 793.
[19] P. Schumacher, K.A.Q. O'Reilly and B. Cantor, in 'Solidification processing 97', Sheffield, (1997), ed. H. Jones and J. Beech, The University of Sheffield, p. 281.
[20] K.A.Q. O'Reilly and B. Cantor, Acta Mater., 43 (1995) 405.
[21] B. McKay, P. Cizek, P. Schumacher and K.A.O' Reilly, Light Metals 2000, ed. R.D. Peterson, (2000), Warrendale, PA, this conference.